International Journal of Applied Earth Observation and Geoinformation 13 (2011) 711–720

Contents lists available at ScienceDirect

International Journal of Applied Earth Observation and Geoinformation

journal homepage: www.elsevier.com/locate/jag

Land use classification from multitemporal Landsat imagery using the Yearly Land Cover Dynamics (YLCD) method

Y. Julien*, J.A. Sobrino, J.-C. Jiménez-Muñoz

Global Change Unit, Image Processing Laboratory, University of Valencia, P.O. Box 22085, E-46071 Valencia, Spain

ARTICLE INFO

Article history:
Received 3 November 2010
Accepted 16 May 2011

Keywords:
Yearly Land Cover Dynamics method
Landsat
Multitemporal
NDVI
Land Surface Temperature

ABSTRACT

Several previous studies have shown that the inclusion of the LST (Land Surface Temperature) parameter to a NDVI (Normalized Difference Vegetation Index) based classification procedure is beneficial to classification accuracy. In this work, the Yearly Land Cover Dynamics (YLCD) approach, which is based on annual behavior of LST and NDVI, has been used to classify an agricultural area into crop types. To this end, a time series of Landsat-5 images for year 2009 of the Barrax (Spain) area has been processed: georeferenciation, destriping and atmospheric correction have been carried out to estimate NDVI and LST time series for year 2009, from which YLCD parameters were estimated. Then, a maximum likelihood classification was carried out on these parameters based on a training dataset obtained from a crop census. This classification has an accuracy of 87% (kappa = 0.85) when crops are subdivided in irrigated and non-irrigated fields, and when cereal crops are aggregated in a single crop, and performs better than a similar classification from Landsat bands only. These results show that a good crop differentiation can be obtained although detailed crop separation may be difficult between similar crops (barley, wheat and oat) due to similar annual NDVI and LST behavior. Therefore, the YLCD approach is suited for vegetation classification at local scale. As regards the assessment of the YLCD approach for classification at regional and global scale, it will be carried out in a further study.

1. Introduction

The vegetation of our planet is changing (IPCC, 2007), due to both direct human action (land use change) and indirect human pressure (greenhouse gases induced global warming). This change is affecting directly food production, with severe consequences for mankind. Therefore, local to global agencies need an adequate monitoring of production, in order to anticipate food shortages, due to droughts for example. To this end, agricultural areas must be classified into different crops, enabling the estimation of areas under a given production. Additionally, monitoring water stress may be needed, to assess the health condition of these crops.

Traditionally, vegetation census has been carried out from vegetation indices, through single date or multitemporal classification (Tucker et al., 1985; Loveland et al., 2000; Morales et al., 2004; Wang and Tenhunen, 2004; Evans and Geerken, 2006; Sobrino et al., 2006). The most widely used vegetation index for this task is the Normalized Difference Vegetation Index (NDVI – Tucker, 1979), which is based on the absorption difference of photosynthetically active tissues in the red and near-infrared wavelengths of the electromagnetical spectrum. Despite its numerous flaws (Holben, 1986), NDVI is the most widely used vegetation index, which is due to its mathematical simplicity, and to the fact that most alternative vegetation indices need additional information which is difficult to obtain at regional and global scale.

As a consequence, several studies have investigated and confirmed the fact that land use assessment and classification as well as vegetation changes could benefit from the addition of the surface temperature to NDVI estimation. For example, Ehrlich and Lambin (1996) used a principal component analysis of BT (Brightness Temperature)/NDVI slopes to build a land cover classification of Africa. Lambin and Ehrlich (1996) reviewed extensively the drivers between NDVI and BT parameters, and described a general spatial pattern of relationships between NDVI and BT, related to land cover. They concluded that BT/NDVI slope could be used to classify land cover and monitor land cover changes over time. Nemani and Running (1997) used BT and NDVI annual variations to build a classification over United States (later extended to the whole globe), and presented an approach to characterize changes in NDVI and BT parameters, which has been used in other studies (Julien et al., 2006). Lambin and Ehrlich (1997) used the results of Lambin and Ehrlich (1996) to build a change index based on NDVI and BT to retrieve change patterns in sub-Saharan Africa. Sobrino and Raissouni (2000) presented two methods for land cover change

* Corresponding author. Tel.: +34 96 354 4054.
E-mail address: yves.julien@uv.es (Y. Julien).

0303-2434/$ – see front matter © 2011 Elsevier B.V. All rights reserved.
doi:10.1016/j.jag.2011.05.008

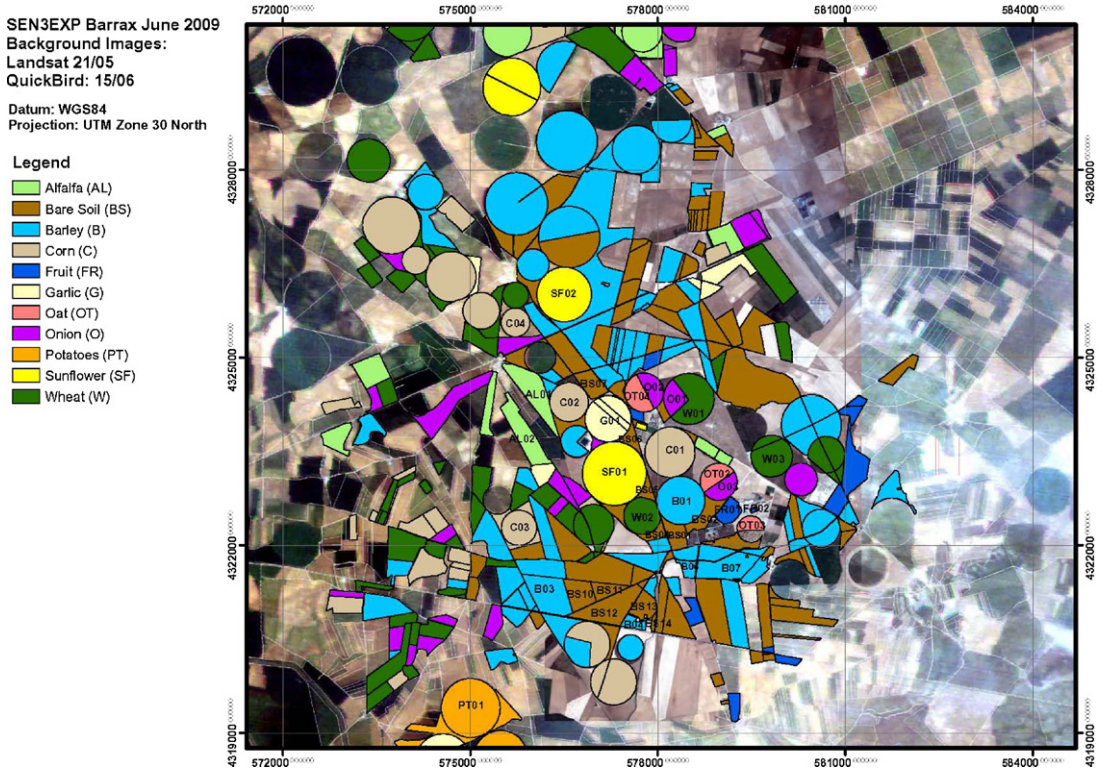

Fig. 1. Description of the study area: Barrax, Albacete, Spain.

detection in Morocco based on NDVI and Land Surface Temperature (LST) temporal variations. Borak et al. (2000) confirmed that coarse resolution estimates of change were best related to fine resolution estimates when BT and NDVI evolutions were considered.

Based on these results, Julien and Sobrino (2009) designed the Yearly Land Cover Dynamics (YLCD) method, which consists in the regression of LST yearly time series against NDVI time series to retrieve three parameters associated with the annual vegetation cycle. These parameters allow distinguishing between broad vegetation categories (Julien and Sobrino, 2009). However, since vegetation species react differently to similar meteorological conditions, mainly through stomata dilatation which in turn depends on leaf characteristics and surface, this method should be able to distinguish between plant species. This is the hypothesis tested in this study, through the use of multitemporal data acquired over an agricultural area in Spain.

2. Study area and data

2.1. Study area

The agricultural area of Barrax (39°3′N, 2°6′W, 700 m) is located in Albacete (Spain). The area has been selected in many other experiments due to its flat terrain, minimizing the complications introduced by variable lighting geometry, and the presence of large, uniform land-use units. Barrax has a Mediterranean type climate, with heavy rainfall in spring and autumn and lower in summer; it presents a high level of continentality, with sudden changes from cold months to warm months and high thermal oscillations in all seasons between the maximum and the minimum daily temperatures (Moreno et al., 2001). The soils of the area are Inceptisols in terms of soil taxonomy, belonging subgroup to Petrocalcic Calcixerepts subgroup (Soil Survey and Staff, 1999). About 65% of cultivated lands at Barrax are dry land (67% winter cereals; 33% fallow) and 35% irrigated land (75% corn; 15% barley/sunflower; 5% alfalfa; 5% onions and vegetables). More details about the test site are presented in Moreno et al. (2001). Fig. 1 presents the study area and the crops used in this study.

2.2. Data

For this study, Landsat images have been provided by the National Geographic Institute of Spain (Instituto Geográfico Nacional – IGN), which has launched the National Plan on Remote Sensing (Plan Nacional de Teledetección – PNT) initiative with the aim of supporting the use of remote sensing in Spain. In the framework of the PNT, Landsat imagery from 2008 to present has been acquired over Spain by the IGN and provided for free to interested users. The IGN also intends to acquire the complete Landsat historical database over the Spanish territory (only some historical Landsat images are currently available). A complete description of the processing of these Landsat images by PNT (geometric, radiometric, atmospheric and topographic corrections) can be found in Peces et al. (2010).

Data from Thematic Mapper (TM) sensor on board Landsat-5 platform have been used in this study. This sensor is widely known by the scientific community, so a detailed description is not provided in this paper. Just as a reminder, TM sensor has four spectral bands in the Visible and Near-InfraRed (VNIR) range (blue, green, red and NIR, corresponding, respectively, to bands 1, 2, 3 and 4), two bands in the Short-Wave InfraRed (SWIR) range (bands 5 and 7) and one band in the Thermal-InfraRed (TIR) range (band 6). Spatial resolution is 30 m for VNIR and SWIR bands and 120 m for TIR band. Bandwidths are around 0.1 μm for VNIR bands, 0.25 μm for SWIR bands and 2 μm for the TIR band.

Since the Barrax site appears in 2 Landsat scenes (corresponding to paths 199 and 200, row 33), a total of 31 images were available from January to December 2009, although only 16 images could be used for this study due to cloud contamination (see Table 1). Data were labeled as cloud contaminated when at least one cloud could

Table 1
Available Landsat images of the study site for year 2009.

Image date	Quality	Observation
13/01/2009	OK	
20/01/2009	Cloudy	Too cloudy to georeference
05/02/2009	Cloudy	Too cloudy to georeference
14/02/2009	OK	
02/03/2009	Cloudy	Too cloudy to georeference
09/03/2009	OK	
03/04/2009	OK	
19/04/2009	Cloudy	Too cloudy to georeference
26/04/2009	Part cloudy	Not used
05/05/2009	OK	
12/05/2009	OK	
21/05/2009	OK	
28/05/2009	Part cloudy	Not used
06/06/2009	Cloudy	Too cloudy to georeference
13/06/2009	OK	
22/06/2009	Part cloudy	Not used
29/06/2009	OK	
15/07/2009	OK	
24/07/2009	OK	
31/07/2009	OK	
09/08/2009	Part cloudy	Not used
16/08/2009	OK	
25/08/2009	Cloudy	Too cloudy to georeference
01/09/2009	OK	
10/09/2009	OK	
17/09/2009	Cloudy	Too cloudy to georeference
26/09/2009	Cloudy	Too cloudy to georeference
13/11/2009	Cloudy	Too cloudy to georeference
20/11/2009	OK	
29/11/2009	Cloudy	Too cloudy to georeference
15/12/2009	Cloudy	Too cloudy to georeference

be identified visually in various RGB compositions of the data by an expert user.

Ancillary data used in this study included a land use map of the test area generated in the framework of the Sen3exp field campaign (ESA, 2010), carried out over the Barrax area in June 2009 and organized by the European Space Agency (ESA) as part of the development process for Sentinel-3 Earth Observation mission, and also MODIS atmospheric products for atmospheric correction purposes, as will be explained below.

3. Methods

This section describes all the operations carried out on the data in this work. These operations include pre-processing, processing and post-processing of the data.

3.1. Pre-processing

First, Landsat images were resized to the Barrax site, destriped (Horn and Woodham, 1979) and then georeferenced to a lat/lon grid using a minimum of 16 ground points chosen from a Google™ Earth image of the Barrax site, with the help of ENVI® software. To this end, specific landscape features were identified in Landsat images by an expert user, and warped to a common lat/lon grid. The resulting images have a dimension of 427 lines and 431 samples, corresponding to longitude and latitude steps of 0°0′30.35″ and 0°0′23.34″, respectively. Then, images were calibrated using radiometric coefficients provided by Chander et al. (2009), and atmospherically corrected using SMAC radiative transfer code (Rahman and Dedieu, 1994).

3.2. Processing

NDVI parameter was estimated from Landsat red (band 3) and infrared (band 4) wavelengths as presented in Eq. (1):

$$\mathrm{NDVI} = \frac{(\mathrm{Band\ 4} - \mathrm{Band\ 3})}{(\mathrm{Band\ 4} + \mathrm{Band\ 3})} \quad (1)$$

As regards LST estimation, the Single-Channel (SC) algorithm developed by Jiménez-Muñoz and Sobrino (2003) and updated to Landsat series in Jiménez-Muñoz et al. (2009) has been applied. Basically, the SC algorithm is based on the radiative transfer equation applied to the Thermal Infra-Red (TIR) band 6 of TM sensor on-board Landsat-5. LST (T_S) is estimated according to:

$$T_S = \gamma \left[\frac{1}{\varepsilon}(\psi_1 L_{\mathrm{sen}} + \psi_2) + \psi_3 \right] + \delta \quad (2)$$

where γ and δ are two parameters computed from at-sensor values (radiance or brightness temperature); ψ_1, ψ_2, and ψ_3 are the atmospheric functions obtained from total atmospheric water vapor contents and ε is the surface emissivity. Details are given in Jiménez-Muñoz et al. (2009). A complete sensitivity analysis of the algorithm to different input data such as water vapor and emissivity is also provided in Jiménez-Muñoz and Sobrino (2003). In this study, water vapor values were extracted from MODIS atmospheric products (MOD05) corresponding to Landsat acquisition dates. Accuracy of MOD05 is better than 0.5 g/cm^2 (or even better, 0.3 g/cm^2 for moderate to low water vapor contents) (Albert et al., 2005). Mean water vapor value provided by MOD05 for the cloud-free dates considered in this study was 1.6 g/cm^2 (with a standard deviation of 0.6 g/cm^2). The single-channel algorithm presented in Eq. (2) provides LST errors between 1 and 2 K for water vapor values ranging between 0.5 and 2 g/cm^2 (Jiménez-Muñoz et al., 2009). Land surface emissivity was estimated using the NDVI thresholds method applied to Landsat5/TM band 6 (see Sobrino et al., 2004, 2008). This method provides errors on retrieved emissivities below 0.015 (Sobrino et al., 2004; Jiménez-Muñoz et al., 2006). Therefore, it is expected that LST be retrieved for the study period with accuracy better than 2 K, even though a rigorous validation could not be performed since in situ measurements were not available.

In order not to lose temporal resolution, the iterative Interpolation Data Reconstruction (IDR – Julien and Sobrino, 2010) method was applied to interpolate cloudy data. However, due to both the concentration of cloudy images in autumn and winter, and the time lapse between two acquisitions (usually reaching one month in autumn and winter months), no satisfactory reconstructed NDVI and LST time series were obtained, and the time series reconstruction had to be discarded.

Then, the YLCD (Julien and Sobrino, 2009) method was applied. This method consists in plotting in the LST/NDVI space the LST and NDVI estimations for all available dates for a given pixel, and then in carrying out a linear regression to retrieve three parameters which describe the yearly behavior of this pixel. Fig. 2 shows how the YLCD parameters are retrieved for a given pixel. First, the pixel LST is normalized between 240 K and 340 K (Normalized Land Surface Temperature – NLST), in order to normalize the NDVI/LST space, as well as to reduce noise levels in NDVI and NLST estimations to comparable levels (around 2% of the signal maximum amplitude). Then, NDVI/NLST trajectory is plotted in this normalized space for the chosen pixel (triangles), and NLST is linearly regressed against NDVI (dotted line). The YLCD parameters are then retrieved: θ is defined as the angle of the regression line with the NDVI axis (related to vegetation type); d as the length of the regression segment (related to vegetation seasonality); and R^2 as the regression coefficient, assessing the adequacy of the linear model to describe vegetation. θ varies between −90° and +90°, with ideal values of 0° for evergreen vegetation, ±90° for bare soils with no vegetation, positive

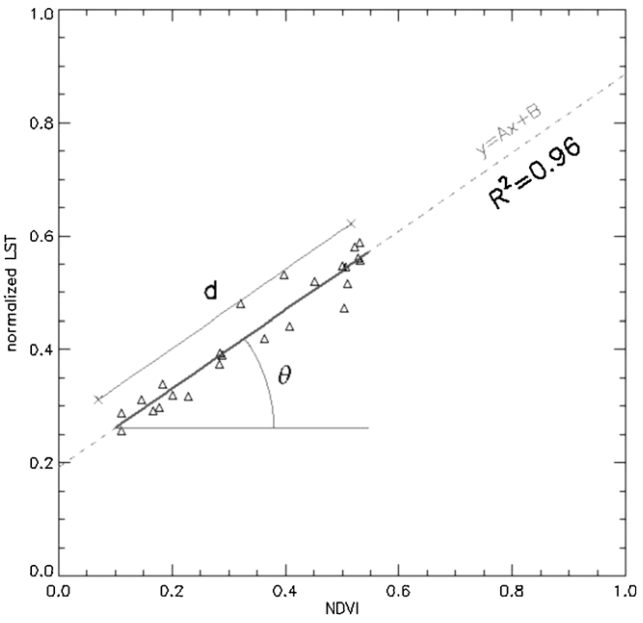

Fig. 2. Retrieval of YLCD parameters (θ, d, R^2) from NDVI and normalized LST for a given pixel. See text for details.

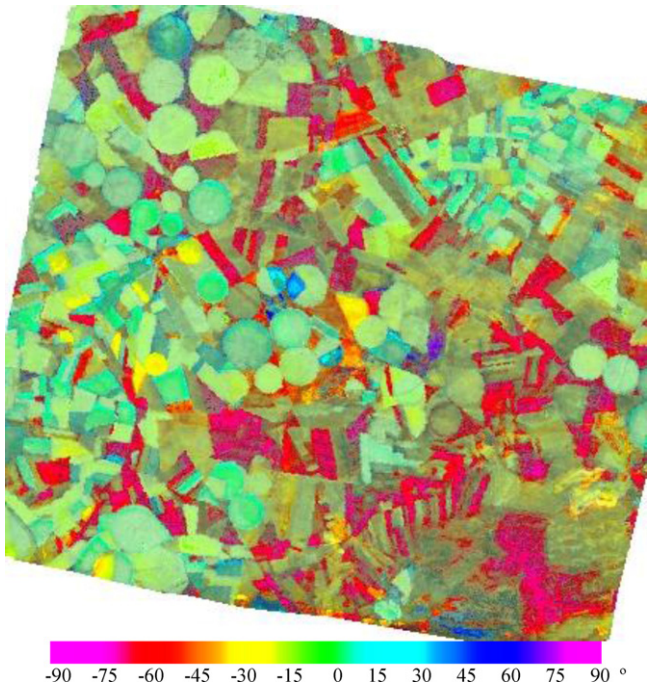

Fig. 3. Yearly Land Cover Dynamics (YLCD) image of the Barrax site. Color bar indicates θ values according to Intensity–Hue–Saturation color composition.

values for temperature or radiation limited vegetation, and negative values for water limited vegetation. d values range between 0 and 1, with low values for vegetation presenting low seasonality (constant NDVI or LST), and high values for high seasonal variations (from snow-covered to fully vegetated surface for example). R^2 values also range between 0 and 1, with low values for noisy NDVI and LST time series (due for example to cloud or atmospheric contamination), and high values for vegetation with highest seasonality, and therefore lower noise. For example, errors of 0.02 for NDVI and NLST for the pixel described in Fig. 2 lead to errors for θ parameter below 2°, a maximum error for d of 0.02, and errors for R^2 around 0.01. More detail on this method can be found in Julien and Sobrino (2009). Since NDVI and LST have different spatial resolutions (30 m and 120 m, respectively), the same LST value was used for the corresponding NDVI pixels.

3.3. Post-processing

In a first step, average NDVI and LST were retrieved for each date for all the nomenclature fields shown in Fig. 1. Since the crop census map is in UTM projection, referenced fields were identified in NDVI and LST images by an expert user. Then, each of these nomenclature fields were parted in two equal areas, one for classification training, and the other for classification validation. Training and validation sample sizes appear in Table 3. A maximum likelihood classification was finally carried out on the three obtained YLCD parameters.

4. Results

This section describes the results obtained regarding both the YLCD procedure and the classification built from the YLCD parameters.

4.1. YLCD approach

Fig. 3 shows the results of the YLCD procedure. The false color image has been obtained through an IHS (Intensity–Hue–Saturation) composition, as described in Julien and Sobrino (2009). When compared with Fig. 1, this figure shows that the YLCD procedure allows a clear distinction between some crops (Alfalfa, Bare Soil, Barley, Garlic, Onion), while some other crops seem more difficult to differentiate (Wheat, Barley and Onion; Sunflower and Corn). From a general point of view, one can observe that the general patterns mentioned in Julien and Sobrino (2009) can also be evidenced here: arid areas (bare soil) appear in red and purple colors, due to the high LST and low NDVI annual amplitudes; species with photosynthetic activity during spring and summer (Sunflower, Corn, Potato) appear in light blue; while species with photosynthetic activity during summer (Onion) appear in dark blue. Semi-arid areas usually appear in yellow, unfortunately the corresponding fields were not referenced during the field campaign, although they probably correspond to unploughed bare soils. All areas in grayish colors correspond to areas for which the linear model fails to represent adequately the NDVI and LST yearly cycle of the vegetation.

Fig. 4 displays the values of all 3 YLCD parameters for the Barrax site. The repartition of θ parameter is presented in Fig. 4(a). This figure shows bare soils with low θ values ($\theta < -50°$), cereal crops (wheat, oat, barley) with negative θ values ($-50 < \theta < -30°$), although these θ values are also found for "greener" crops (onion, garlic), due to the fact that the pixel proportion of bare soil for these latter crops is high. On another hand, green crops (corn, sun flower, potato, alfalfa) have positive θ values, with sometimes values close to 0, which may be surprising since NDVI is expected to vary from sowing to harvest. This can be explained by the high proportion of clouds during winter, during which these fields are bare, and therefore eliminated from the analysis. Fig. 4(b) presents the distribution for d parameter. This figure shows that d values range mainly between 0.1 and 0.5. Once again, bare soils can be easily identified ($0.1 < d < 0.2$), while most crops have superior values ($0.2 < d < 0.5$), with generally higher d values for wheat and barley, slightly lower for corn, sun flower and potato. Alfalfa crops show low d values ($0.1 < d < 0.2$), which can be explained by the fact that these crops are partially harvested several times a year, resulting in low NDVI variations. Finally, Fig. 4(c) presents R^2 values for the Barrax site. These R^2 values span the whole parameter range [0,1], with some inhomogeneities within fields. Lowest R^2 values are obtained for potato crop ($0 < R^2 < 0.1$), followed by sun flower ($0 < R^2 < 0.3$), alfalfa

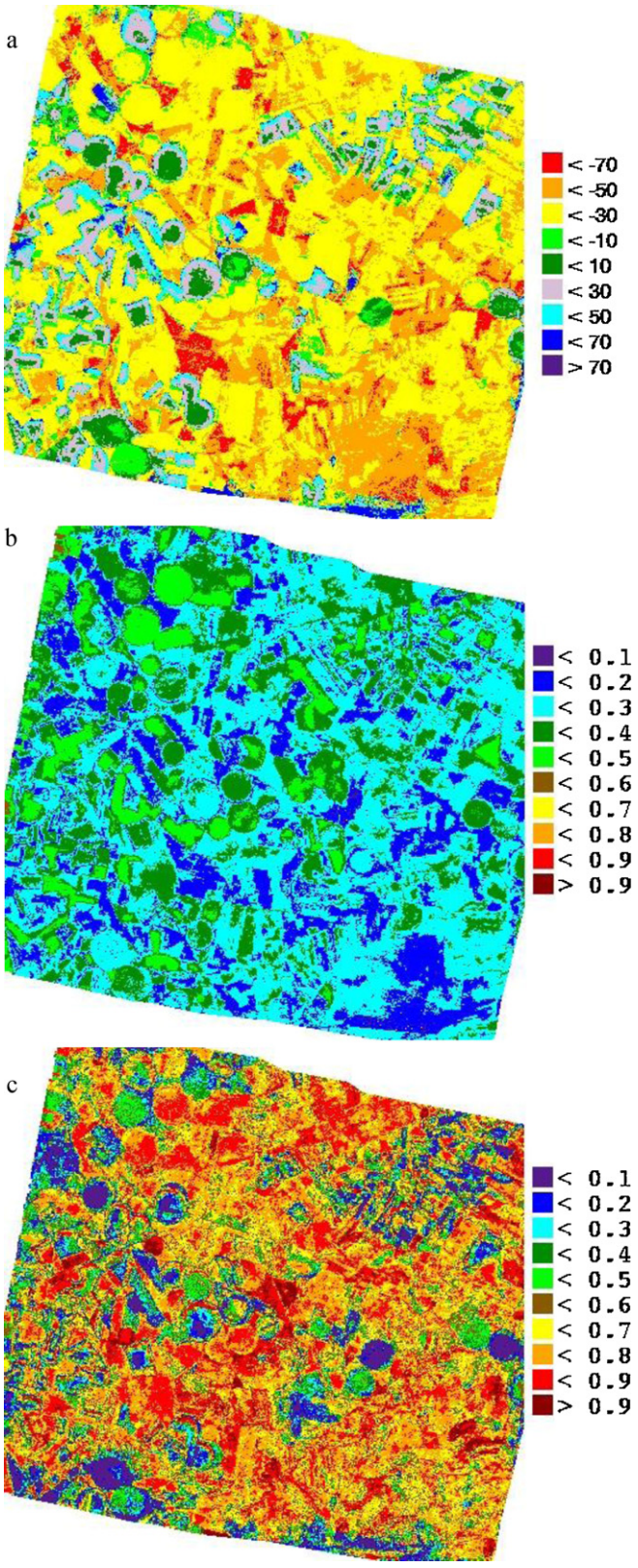

Fig. 4. Yearly land cover dynamics (YLCD) parameters as retrieved at Barrax site: (a) θ, (b) d, and (c) R^2.

Table 2
YLCD parameter characteristics for all referenced fields (see Fig. 1).

	θ		d		R^2	
	$E(X)$	σ_X	$E(X)$	σ_X	$E(X)$	σ_X
AL01	−12.3	4.1	0.54	0.04	0.09	0.06
AL02	−3.1	3.3	0.52	0.03	0.01	0.02
B01	−11.4	3.2	0.69	0.03	0.12	0.05
B03	−24.2	3.4	0.55	0.04	0.16	0.04
B07	−21.5	5.8	0.40	0.03	0.08	0.03
BS07	−69.8	4.1	0.51	0.01	0.50	0.10
BS10	−67.5	5.7	0.49	0.02	0.32	0.15
BS12	−67.4	5.4	0.48	0.03	0.28	0.12
C01	7.3	3.8	0.69	0.05	0.12	0.08
C02	12.0	3.9	0.71	0.03	0.38	0.13
C03	8.7	2.2	0.72	0.02	0.25	0.08
C04	14.2	3.8	0.69	0.03	0.43	0.11
FR01	−48.6	11.1	0.43	0.05	0.24	0.11
G01	−14.7	3.8	0.46	0.03	0.06	0.03
O01	41.1	5.2	0.49	0.05	0.62	0.15
O02	29.1	5.6	0.53	0.04	0.47	0.10
O03	30.2	6.6	0.49	0.04	0.42	0.12
OT02	−5.6	3.7	0.66	0.03	0.03	0.04
OT03	−7.0	2.0	0.70	0.04	0.04	0.02
OT04	−3.3	2.6	0.67	0.03	0.02	0.01
PT01	2.2	3.5	0.70	0.02	0.03	0.05
SF01	8.9	5.6	0.59	0.05	0.11	0.10
SF02	8.2	5.1	0.67	0.03	0.14	0.12
W01	−7.8	3.5	0.67	0.04	0.06	0.05
W02	−13.3	1.7	0.73	0.02	0.13	0.03
W03	−14.3	3.0	0.70	0.03	0.14	0.07

$E(X)$ = average value.
σ_X = standard deviation.

($0 < R^2 < 0.4$), corn ($0 < R^2 < 0.5$), garlic ($0.4 < R^2 < 0.5$), while cereals (barley, wheat and oat), onion and bare soils present higher values ($0.8 < R^2 < 1$).

In order to estimate if these differences are sufficient for building a land use classification from YLCD parameters, average and standard deviations have been estimated for all YLCD parameters and all referenced fields in Fig. 1. These statistics are presented in Table 2. This table shows that statistics are similar within crops, showing good crop homogeneity over different fields, except in the case of Alfalfa, Barley, Onion and Wheat. These latter crops may exhibit these differences to different irrigation schemes, resulting in slightly different crop phenologies. Additionally, the Fruit Tree field shows an abnormally high standard deviation in θ parameter, which is due to the fact that this field consisted in young pistachio trees (separated by 3 m) surrounded by bare soil, with an estimated fractional vegetation cover lower than 10%. Therefore, at a 30 m resolution, each pixel includes both pistachio trees and bare soil in variable proportions. Table 2 also shows that some crops may be difficult to distinguish from others. For example, W02, W03, G01 and B01 present similar characteristics, while SF01 and SF02 YLCD parameter range is included in the variability range of corn fields (C01, C02, C03 and C04).

4.2. Classification

The study area has been classified from YLCD parameters through a maximum likelihood classification, using all labeled fields in Fig. 1 to generate crop statistics. In order to increase the accuracy of the classification, two additional classes were created, corresponding to non-irrigated barley (B03 and B07) and non-irrigated wheat (blue rectangular fields, not referenced in Fig. 1). Only half of the pixels of each labeled field has been used for the classification, the other half being spared for validation purposes. The obtained classification is presented in Fig. 5. This classification shows that, as expected, some crops are misclassified, for example Corn and Potato; Barley and Wheat; or Bare Soil and Fruit Trees. The

Table 3
Confusion matrix for the classification obtained from YLCD parameters.

Class	Alfalfa	Barley	Bare Soil	Corn	Fruit Tree	Garlic	Onion	Oat	Potato	Sunflower	Wheat	Wheat NI	Barley NI	Total
Alfalfa	**174**	3	0	0	0	0	0	3	0	1	3	0	0	184
Barley	0	**511**	0	0	0	0	0	2	0	0	124	95	0	732
Bare Soil	0	0	**475**	0	2	0	0	0	0	0	0	0	0	477
Corn	0	0	0	**336**	0	0	0	0	15	83	0	0	0	434
Fruit Tree	0	0	5	0	**12**	0	0	0	0	0	0	0	0	17
Garlic	0	0	0	0	0	**134**	0	0	0	0	0	0	52	186
Onion	0	0	0	0	0	0	**178**	0	0	1	0	0	0	179
Oat	2	118	0	1	0	0	0	**104**	3	2	104	9	0	343
Potato	0	6	0	107	0	0	0	10	**283**	115	0	0	0	521
Sunflower	8	0	0	44	0	0	5	1	12	**416**	0	0	0	486
Wheat	1	113	0	0	0	0	0	5	0	0	**149**	29	0	297
Wheat NI	0	109	0	0	0	0	0	0	0	0	12	**123**	0	244
Barley NI	1	6	0	0	6	4	0	1	0	0	0	0	**254**	272
Total	186	866	480	488	20	138	183	126	313	618	392	256	306	4372

NI = non-irrigated.

confusion between Bare Soil and Fruit Tree is easy to understand, since, as explained above, Fruit Tree fields consist of isolated trees on a bare soil. From the YLCD parameter statistical analysis carried above, the misclassification of Barley and Wheat is not surprising either. As regards the confusion between Corn and Potato, it is due to their similarity in d and R^2 parameters, combined with a small difference in θ parameter. For example, W01 field appears wrongly as a juxtaposition of Wheat, Onion and Barley crops. Excepting these few exceptions, the classification shows a good homogeneity within field units.

Table 3 shows the confusion matrix corresponding to the classification. This confusion matrix was obtained by comparison of the YLCD parameter classification with the validation data mentioned above. For this confusion matrix, two types of crops were added to the ones presented above, in order to differentiate between irrigated and non-irrigated barley and wheat fields. For example, B01 is an irrigated barley field, while B03 and B07 are not irrigated. This difference explains the difference shown in Table 2 as regards YLCD parameter statistics by field. The kappa coefficient for this classification is 0.69, and the classification accuracy is 72%.

5. Discussion

The kappa coefficient obtained by this classification shows that some crops are not identified correctly. Fig. 6 shows NDVI and LST evolutions for year 2009 for all the referenced fields. Fig. 6a1 shows that alfalfa fields are harvested several times a year, which explains

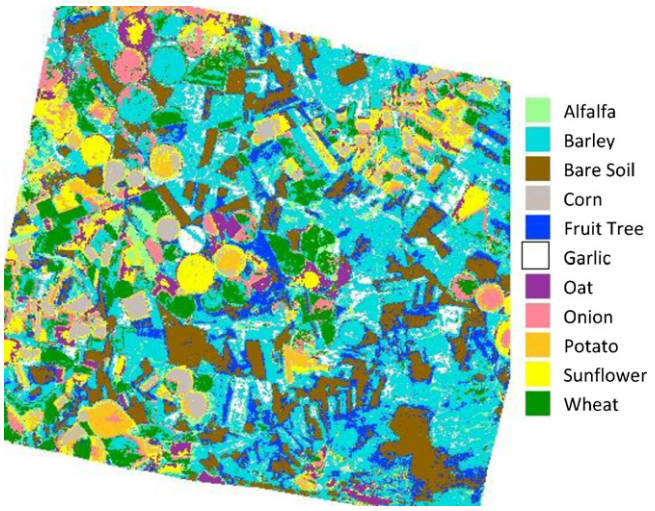

Fig. 5. Classification of the Barrax site based on the YLCD parameters.

the low R^2 value obtained from the YLCD procedure for this crop. Moreover, this same graph shows that harvesting dates can differ (last harvest day of year 228 for AL01 and 244 for AL02), and therefore diminishes the intra-class coherence of the training and validation data. As observed above, some crops have almost identical NDVI and LST annual evolution (W01, W02, W03 and B01 on one hand; SF01, SF02, C01, C02, C03 and C04 on the other). On the contrary, barley crops do not show the same NDVI behavior. This is explained by the fact that B01 field is pivot-irrigated, while B03 and B07 fields are not irrigated, and therefore these fields are more subject to water stress, which results in a lesser development of the plants. Wheat (W01, W02 and W03) and barley (B01) crops have very similar plant structure and phenology, reinforced by the similar irrigation pattern applied to them. The same observation is valid for sunflower and corn crops, which also present the peculiarity of a flat summer LST profile, due to their high foliage density which allow them to regulate their temperature by stomatal evapotranspiration.

We merged irrigated wheat and barley crops in the same class, and carried out a maximum likelihood classification scheme as described above. The kappa coefficient obtained with this classification is 0.79, with classification accuracy above 82%. If we merge all irrigated cereal crops (barley, wheat and oat) in a single class, the resulting classification present a kappa coefficient of 0.85, and classification accuracy above 87%. This shows that the YLCD approach is useful for classifying crops, although similar plants cannot be differentiated by this method.

Due to Landsat sensor characteristics, NDVI and LST data are not retrieved at the same resolution: channels 3 and 4 have a ground resolution of 30 m, which results (Eq. (1)) in an estimation of NDVI at 30 m, while LST is estimated at 120 m ground resolution. However, Goetz (1997) demonstrated that the NDVI/LST relationship is stable over different spatial resolutions, so the difference in spatial resolution between NDVI and LST should not affect the results presented here.

As mentioned in the previous section, different phenologies within the same crop (although in different fields, with possibly different irrigation schemes) may decrease the separability between classes, through a larger dispersion of the YLCD parameters within a same class. For example, a delay in irrigation may cause smaller leaves than expected, resulting in lower NDVI value and higher LST (due to a lesser evapotranspiration), which would lead to changes in θ, d, and R^2 values. Additionally, inhomogeneities for Fruit Tree fields increase the error in classification since part of this crop can be described as bare soil.

In order to assess the validity of the YLCD-based classification, a more conventional classification has been conducted directly on Landsat data. To this end, Landsat image for 29 June 2009 was

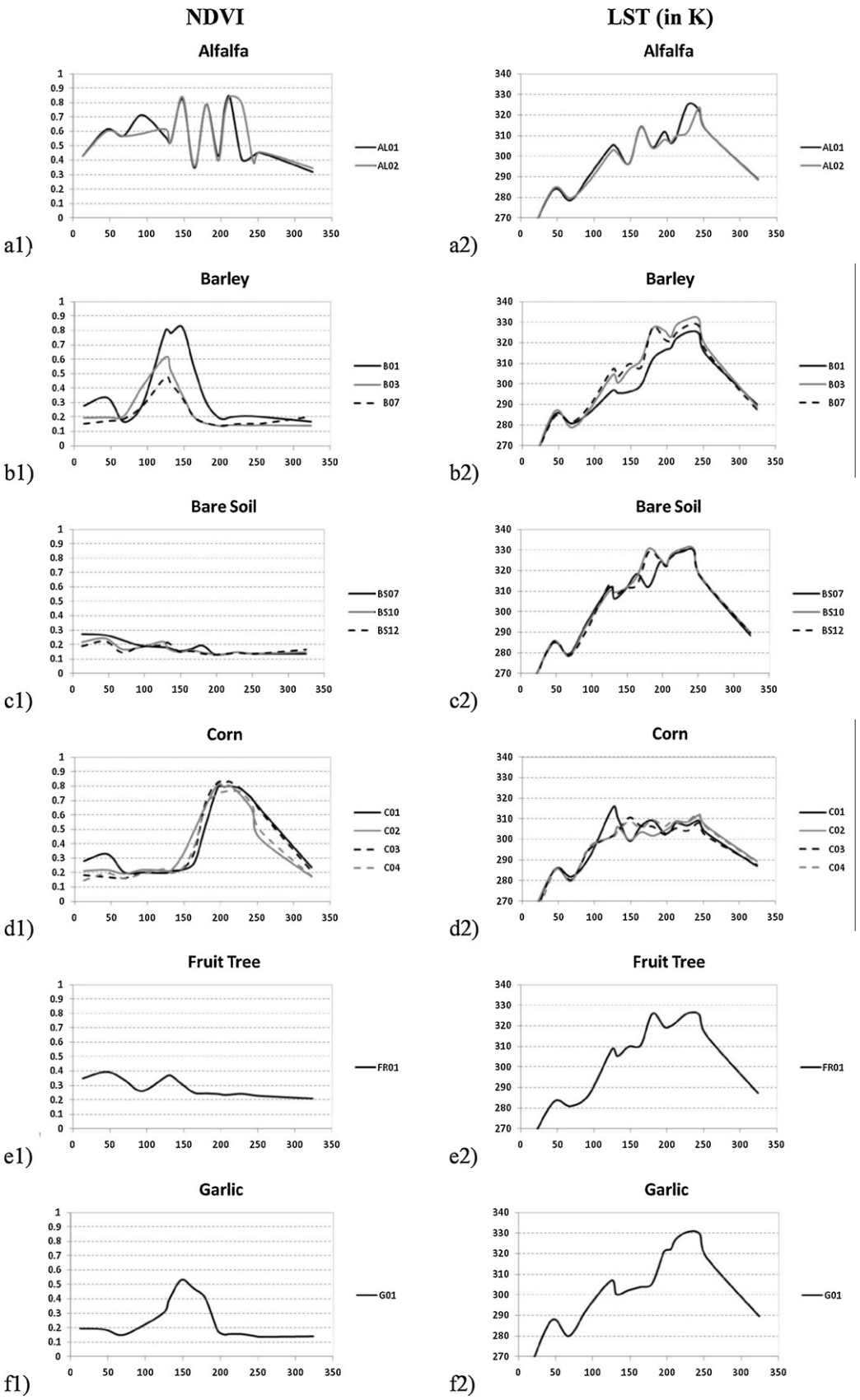

Fig. 6. Description of NDVI and LST trajectories for various crops and land uses. Description of NDVI and LST trajectories for various crops and land uses.

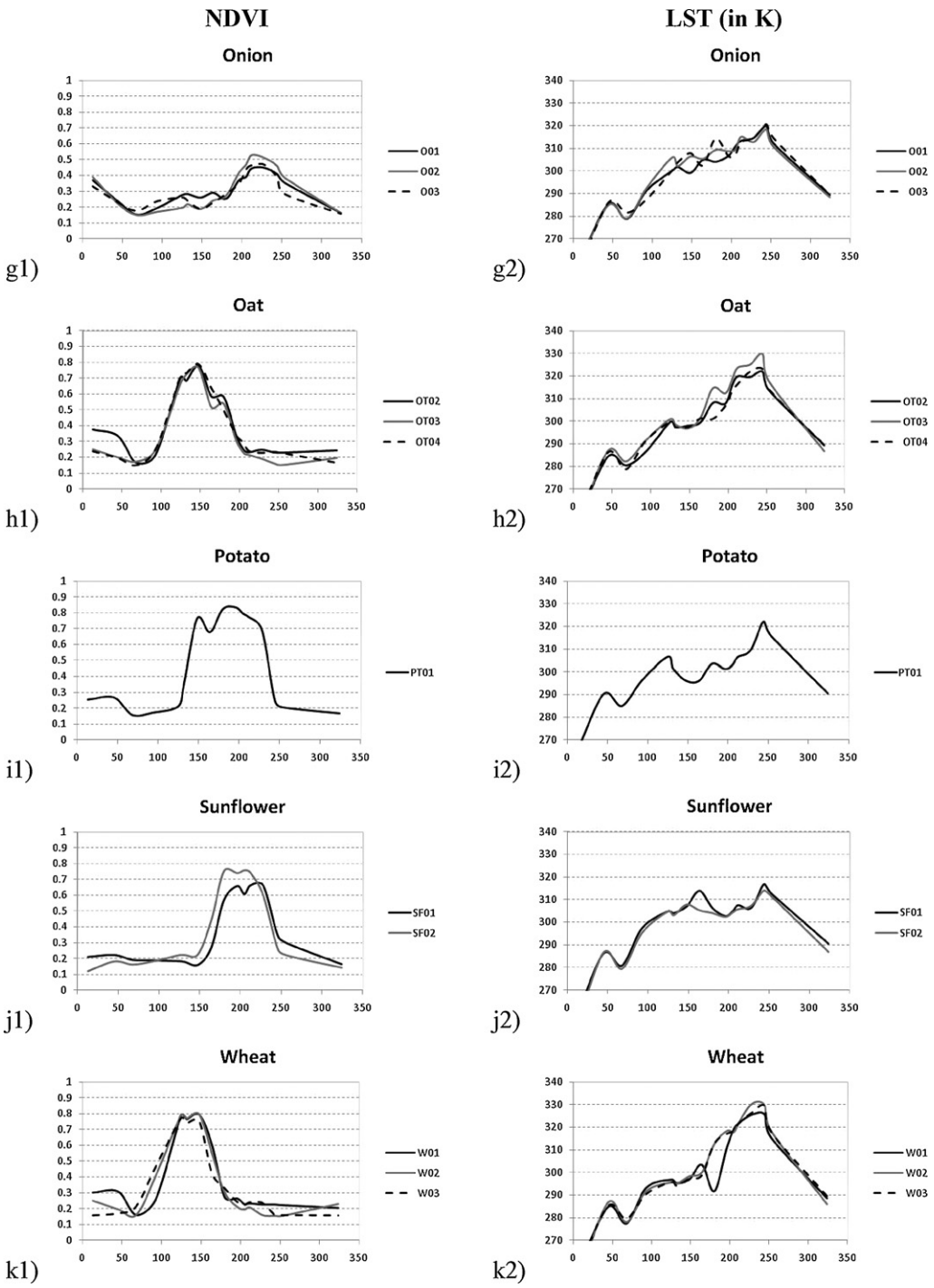

Fig. 6. (*Continued*).

chosen, since this date corresponds to vegetation activity for most crops (see NDVI curves in Fig. 6). A maximum likelihood classification was conducted on all 7 bands, using the same training and validation pixels as for the YLCD classification. This classification is shown in Fig. 7. This classification presents a kappa value of 0.68, with an overall accuracy of 71%. When merging all irrigated cereal crops as done for YLCD classification, kappa value increases to 0.80, and overall accuracy to 82%. Therefore, the YLCD classification performs slightly better than a traditional Landsat classification, although when comparing Figs. 3 and 5, some bare field delimitations are clearer for the traditional Landsat classification, due to the confusion of the YLCD classification between bare soil and fruit trees.

Ehrlich and Lambin (1996) obtained classification accuracies between 75% and 85% with their BT/NDVI slope method depending on the chosen validation dataset. Nemani and Running (1997) managed to obtain classification accuracy above 90% when using broad classes, which decreased to 73% when using more specific classes. It should be mentioned that these works used broad classes for regional classification, while the work presented here relies on crop differentiation, which is obtained satisfactorily when differentiating between irrigated and non-irrigated crops, and when merging

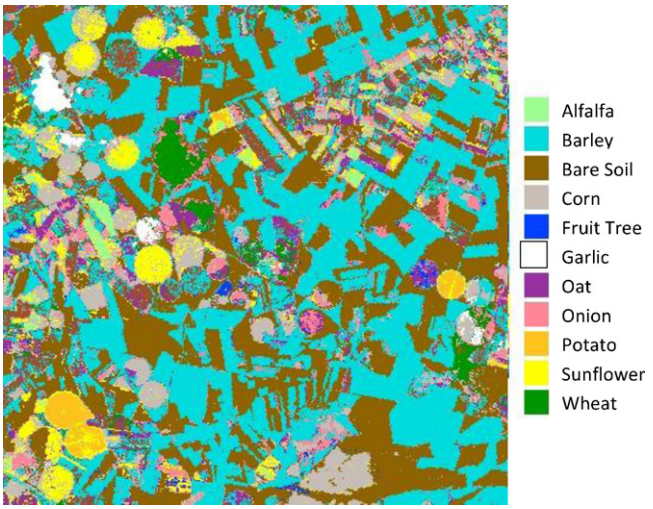

Fig. 7. Classification of the Barrax site based on all 7 Landsat bands for 29 June 2009.

all cereal crops in the same class. Therefore, when using the YLCD method for vegetation classification, one has to keep in mind that this method is based on annual LST and NDVI evolutions, and that the differentiation between crops with similar LST and NDVI annual behaviors may be difficult. The results presented here show that when the method is applied in agreement with this observation, it yields good results in crop differentiation.

6. Conclusion

This paper has described a methodology to classify crop vegetation through the use of the Yearly Land Cover Dynamics (YLCD) method, which is based on the annual behavior of NDVI and LST parameters. When applied to an agricultural site, this approach allows an accurate classification of the represented fields, although cereal cultures had to be merged in a single class due to their similarity. Additionally, irrigated and non-irrigated crops had to be separated in different classes due to strong differences in NDVI and LST annual behaviors.

These results show that the YLCD approach is suited for vegetation classification at local scale, and therefore could be used to monitor and assess land cover change at local scale, through a yearly classification of a given area such as the agricultural site chosen in this study. As regards the ability of the YLCD approach to monitor and assess land cover change at broader scale (regional to global), it will be explored by the authors in a near future.

Acknowledgements

The authors would like to thank the Laboratory for Earth Observation (LEO) group of the University of Valencia for providing the Barrax field nomenclature image, Jordi Cristóbal (CREAF-Autonomous University of Barcelona) for assistance with Landsat radiometric calibration issues and the Instituto Geográfico Nacional (IGN, Spain) for providing Landsat imagery. The authors also wish to thank the European Union (CEOP-AEGIS, Project FP7-ENV-2007-1, Proposal No. 212921; WATCH, Project 036946) and the Ministerio de Ciencia y Tecnología (EODIX, Project AYA2008-0595-C04-01) for their financial support.

References

Albert, P., Bennartz, R., Preusker, R., Leinweber, R., Fischer, J., 2005. Remote sensing of atmospheric water vapor using the moderate resolution imaging spectroradiometer. Journal of Atmospheric and Oceanic Technology 22, 310–314.
Borak, J.S., Lambin, E.F., Strahler, A.H., 2000. The use of temporal metrics for land cover change detection at coarse spatial scales. International Journal of Remote Sensing 21 (6 & 7), 1415–1432.
Chander, G., Markham, B.L., Helder, D.L., 2009. Summary of current radiometric calibration coefficients for Landsat MSS, TM, ETM+, and EO-1 ALI sensors,. Remote Sensing of Environment 113, 893–903.
Ehrlich, D., Lambin, E.F., 1996. Broad scale land-cover classification and interannual climatic variability. International Journal of Remote Sensing 17 (5), 845–862.
ESA, 2010. Sentinel 3 Experimental campaign, Final Report, ESA, p. 294.
Evans, J.P., Geerken, R., 2006. Classifying rangeland vegetation type and coverage using a Fourier component based similarity measure. Remote Sensing of Environment 105, 1–8.
Goetz, S.J., 1997. Multi-sensor analysis of NDVI surface temperature and biophysical variables at a mixed grassland site. International Journal of Remote Sensing 18 (1), 71–94.
Holben, B.N., 1986. Characteristics of maximum-value composite image from temporal AVHRR data. International Journal of Remote Sensing 7, 1417–1434.
Horn, B.K.P., Woodham, R.J., 1979. Destriping LANDSAT MSS images by histogram modification. Computer Graphics and Image Processing 10, 69–83.
IPCC, 2007. Climate change 2007: the physical science basis – Summary for policymakers, IPCC Fourth Assessment Report.
Jiménez-Muñoz, J.C., Sobrino, J.A., 2003. A generalized single-channel method for retrieving land surface temperature from remote sensing data. Journal of Geophysical Research 108 (D22), doi:10.1029/2003JD003480.
Jiménez-Muñoz, J.C., Sobrino, J.A., Gillespie, A., Sabol, D., Gustafson, W.T., 2006. Improved land surface emissivities over agricultural areas using ASTER NDVI. Remote Sensing of Environment 103, 474–487.
Jiménez-Muñoz, J.C., Cristóbal, J., Sobrino, J.A., Sória, G., Ninyerola, M., Pons, X., 2009. Revision of the single-channel algorithm for land surface temperature retrieval from Landsat thermal-infrared data. IEEE Transactions on Geoscience and Remote Sensing 47 (1), 339–349.
Julien, Y., Sobrino, J.A., 2009. The yearly land cover dynamics (YLCD) method: an analysis of global vegetation from NDVI and LST parameters. Remote Sensing of Environment 113, 329–334.
Julien, Y., Sobrino, J.A., 2010. Comparison of cloud-reconstruction methods for time series of composite NDVI data. Remote Sensing of Environment 114, 618–625.
Julien, Y., Sobrino, J.A., Verhoef, W., 2006. Changes in land surface temperatures and NDVI values over Europe between 1982 and 1999. Remote Sensing of Environment 103, 43–55.
Lambin, E.F., Ehrlich, D., 1996. The surface temperature-vegetation index space for land cover and land-cover change analysis. International Journal of Remote Sensing 17 (3), 163–487.
Lambin, E.F., Ehrlich, D., 1997. Land-cover changes in sub-Saharan Africa (1982–1991): application of a change index based on remotely sensed surface temperature and vegetation indices at a continental scale. Remote Sensing of Environment 61, 181–200.
Loveland, T.R., Reed, B.C., Brown, J.F., Ohlen, D.O., Zhu, Z., Yang, L., Merchant, J.W., 2000. Development of a global land cover characteristics database and IGBP DIS Cover from 1 km AVHRR data. International Journal of Remote Sensing 21 (6 & 7), 1303–1330.
Morales, L., Castellaro, G., Sobrino, J.A., El Kharraz, J., 2004. Land cover dynamic monitoring in the region of Coquimbo (Chile) by the analysis of multitemporal NOAA-AVHRR NDVI images. In: ISPRS Conference, Commission VI, 12–23 July 2004, Istanbul, Turquia.
Moreno, J., Caselles, V., Martínez-Lozano, J.A., Meliá, J., Sobrino, J.A., Calera, A., Montero, F., Cisneros, J.M., 2001. The Measurements Programme at Barrax, DAISEX Final Results Workshop, ESTEC, Holland, 15–16 March ,. ESA Publications Division, SP-499, pp. 43–51.
Nemani, R.R., Running, S.W., 1997. Land cover characterization using multitemporal red, near-IR, and thermal-IR data from NOAA/AVHRR. Ecological Applications 7 (1), 79–90.
Peces, J.J., Villa, G., Arozarena, A., Tejeiro, J.A., Domenech, E., Plaza, N., 2010. Spanish National Remote Sensing Program, a way to achieve massive use of remote sensing data. In: 3rd International Simposium in Quantitative Remote Sensing, Proceedings of the 3rd International Symposium in Quantitative Remote Sensing, 27 Septiembre–1 Octubre 2010, Torrent, Valencia, Spain, pp. 477–482, ISBN: 978-84-370-7952-3.
Rahman, H., Dedieu, G., 1994. SMAC: a simplified method for the atmospheric correction of satellite measurements in the solar spectrum. International Journal of Remote Sensing 15 (1), 123–143.
Sobrino, J.A., Raissouni, N., 2000. Toward remote sensing methods for land cover dynamic monitoring: application to Morocco. International Journal of Remote Sensing 21 (2), 353–366.
Sobrino, J.A., Jiménez-Muñoz, J.C., Paolini, L., 2004. Land surface temperature retrieval from LANDSAT TM 5. Remote Sensing of Environment 90, 434–440.
Sobrino, J.A., Julien, Y., Morales, L., 2006. Multitemporal analysis of PAL images for the study of land cover dynamics in South America. Global and Planetary Change 51, 172–180.
Sobrino, J.A., Jiménez-Muñoz, J.C., Sòria, G., Romaguera, M., Guanter, L., Moreno, J., Plaza, A., Martínez, P., 2008. Land surface emissivity retrieval from different VNIR

and TIR sensors. IEEE Transactions on Geoscience and Remote Sensing 48 (2), 316–327.
Soil Survey Staff, 1999. Soil Taxonomy. A Basic System of Soil Classification for Making and Interpreting Soil Surveys, Agriculture Handbook No. 466, second ed. USDA, Washington, USA.
Tucker, C.J., 1979. Red and photographic infrared linear combinations for monitoring vegetation. Remote Sensing of Environment 8 (2), 127–150.
Tucker, C.J., Townshend, J.R.G., Goff, T.E., 1985. African land-cover classification using satellite data. Science 227 (4685), 369–375.
Wang, Q., Tenhunen, J.D., 2004. Vegetation mapping with multitemporal NDVI in North Eastern China Transect (NECT). International Journal of Applied Earth Observation and Geoinformation 6, 17–31.